Radiation shielding of high-energy neutrons in SAD

P. Seltborg[1], A. Polanski[2], S. Petrochenkov[2], A. Lopatkin[3], W. Gudowski[1], V. Shvetsov[2]

[1]*Department of Nuclear and Reactor Physics*
Albanova University Centre, Royal Institute of Technology
S-106 91 Stockholm, Sweden

[2]*Joint Institute for Nuclear Research*
141 980, Joliot-Curie 6, Dubna, Russia

[3]*Research and Development Institute of Power Engineering*
101 000, PB78, Moscow, Russia

Abstract

The radiation fields and the effective dose at the Sub-critical Assembly in Dubna (SAD) have been studied with the Monte Carlo code MCNPX. The effective dose above the shielding, i.e. in the direction of the incident proton beam of 3.0 μA, was found to be about 190 μSv/h. This value meets the dose limits according to Russian radiation protection regulations, provided that access to the rooms in this area is not allowed for working personnel during operation.

By separating the radiation fields into a spallation-induced and a fission-induced part, it was shown that the neutrons with energy higher than 10 MeV, originating exclusively from the proton-induced spallation reactions in the target, contribute for the entire part of the radiation fields and the effective dose at the top of the shielding. Consequently, the effective dose above the SAD reactor system is merely dependent on the proton beam properties and not on the reactivity of the core.

Keywords: SAD; Effective dose; MCNPX; high-energy neutrons; sub-critical; ADS

1. Introduction

In the up-coming SAD experiments [1, 2], set up at the Joint Institute for Nuclear Research in Dubna (JINR) in collaboration with CEA (Cadarache), CIEMAT (Madrid), FZK (Karlsruhe) and KTH (Stockholm), the various concepts and the basic physical principles of accelerator-driven systems (ADS) [3-5] will be studied extensively. In these experiments, a 660 MeV proton accelerator is coupled to a sub-critical core, loaded with fast reactor MOX (Mixed Oxide) fuel assemblies. The proton beam impinges on a target of lead, which generates a large number of neutrons via spallation reactions. The produced spallation neutrons leak out from the target, thus providing the sub-critical core with a strong external neutron source.

A major concern before licensing the operation of SAD is to accurately determine the radiation fields outside the reactor system. The surrounding building is shielded from the radiation emerging from the accelerator beam and the reactor by thick walls of concrete. In the present paper, the effective dose induced in the rooms above the reactor, i.e. in the direction of the incident proton beam, have been determined in order to verify that they do not exceed the limits determined by the Russian radiation protection regulations. The studies have been quantified by first calculating, with the Monte Carlo code MCNPX [6], the flux of the particles leaking out through the shielding and then by converting the obtained fluxes to effective dose. The effective doses have been obtained by using fluence-to-effective dose conversion coefficients, provided mainly by the International Commission for Radiological Protection (ICRP) [7] and the International Commission on Radiation Units (ICRU) [8].

The shielding problems in a system coupled to a high-energy proton beam are mainly connected to the deeply penetrating high-energy neutrons. These neutrons, released in the spallation process by direct head-on collisions between the source protons and the target nuclei (the intranuclear cascade phase), have a strong angular dependence and can, in the forward direction, reach energies up to the level of the incident protons [9, 10]. The lower-energy neutrons, on the other hand, created in the subsequent evaporation stage and emitted nearly isotropically, constitute only a minor shielding concern, due to their comparatively short range in most shielding materials. For this reason, the largest radiation doses will appear in the forward direction of the incident proton beam [11] and the design of the biological shielding in this direction will generally be of largest importance. The objective of the present paper has been to study the radiation fields and the effective dose where they are maximal, i.e. above the reactor.

In the following section, a brief introduction to the quantities and conversion coefficients used for radiologi-

cal protection against external radiation is first given, followed by a description of the SAD experiments and the calculation method that was applied in the study. In Section 4, the results from the simulations are presented and analysed, with special focus given to the effects coming from the high-energy neutrons. First, the particles entering into the biological shielding are studied in terms of flux and energy spectra. The effective dose and the energy spectra of the particles detected at the top of the shielding are then determined. The next sub-section addresses the transport and the attenuation of the particles in the shielding. Then, the relative contribution to the effective dose from high-energy neutrons and low-energy neutrons are studied and finally, the design of the biological shielding is optimised in order to reduce the dose to the Russian radiation limits for working personnel.

2. Conversion coefficients for use in radiological protection

2.1. Radiological protection quantities

There are three principal protection quantities currently recommended for use in radiological protection [7, 8]; the mean absorbed dose in an organ or tissue (D_T), the equivalent dose in an organ or tissue (H_T) and the effective dose (E).

2.1.1. Absorbed dose

The absorbed dose, D_T [J/kg or Gy], in a particular organ or tissue, T, in the human body is given by

$$D_T = \frac{1}{m_T} \cdot \int_T D \cdot dm \,, \tag{1}$$

where m_T is the mass of the organ or tissue and D is the absorbed dose in the mass element *dm*.

2.1.2. Equivalent dose

In order to calculate the equivalent dose, H_T, in an organ or tissue, the radiation field in which the organ is present must be divided into energy bins and into the different types of radiation that the field consists of. The absorbed dose in the organ of each radiation bin, $D_{T,R}$, must then be multiplied by a radiation-weighting factor, w_R, and summed over the different radiations, R, i.e.,

$$H_T = \sum_R w_R \cdot D_{T,R} \,. \tag{2}$$

2.1.3. Effective dose

The effective dose, E, was introduced for the quantification of the medical risk from a given radiation exposure. E is defined as the sum of the tissue-weighted equivalent doses in all the tissues and organs of the body,

$$E = \sum_T w_T \cdot H_T \,, \tag{3}$$

where w_T is the tissue-weighting factor for tissue T. For the purpose of radiological protection calculations, the human body is in the ICRP Publication 60 [12] defined by 12 designated tissues and organs plus the remainder, which consists of 10 additional tissues and organs.

2.2. Fluence-to-effective dose conversion coefficients

In order to calculate the effective dose induced by any particle flux, the fluence-to-effective dose conversion coefficients for all energies of all particle types that may be present in the radiation field should be known. Using this set of conversion coefficients together with the specific particle flux that a person may be exposed of, the effective dose received by that person could be determined. The fluence-to-effective dose conversion coefficients are determined by calculating the total effective dose in an anthropomorphic model representing the human body, for mono-energetic fields of all particles of interest. The resulting effective dose for each energy bin is then divided by the total fluence of each radiation.

A number of studies determining these conversion coefficients have been performed by different research groups, using different simulation tools (mainly Monte Carlo codes) and different anthropomorphic models for the radiation transport calculations. In the ICRU Report 57, the results from many of the relevant studies are summarized. Most of the calculations of protection quantities reviewed were made with an adult model using either a hermaphrodite MIRD-5 phantom [13] or modified MIRD-based phantoms, e.g. ADAM and EVA [14], with sex-specific differences. The data points from each group of authors were combined into one data set for each organ as a function of particle energy, resulting in one combined data set for each organ and for each gender. The conversion coefficients for the effective dose per unit fluence for whole-body irradiation by neutrons in isotropic irradiation geometry (ISO), recommended by the ICRU Report 57, cover the range from thermal energies up to 20 MeV. However, for dose calculations around an ADS driven by high-energy protons, such as the SAD experiments, conversion coefficients up to the energy of the incident protons are needed.

In the present study, the fluence-to-effective dose coefficients for neutrons from thermal neutrons up to 20 MeV are taken from the ICRU Report 57. For neutrons with energy from 20 up to 500 MeV, as well as for photons and protons of all energies, the coefficients are taken from a study by V. Mares and H. Schraube [15]. The calculations presented in [15] were performed with the high-energy Monte Carlo code MCNPX, using the ADAM and EVA anthropomorphic models. The results from Mares and Schraube were also found to be in good agreement with the overview of fluence-to-effective dose conversion coefficients for high-energy radiation performed by M. Pelliccioni [16]. All fluence-to-effective dose conversion coefficients used in the study were based on the ISO geometry and are listed in Table A.1.

3. System modelling

3.1. The SAD design

The conceptual design of the SAD facility is based on a sub-critical highly enriched MOX-loaded core, driven by a 660 MeV proton beam impinging on a target of lead. The protons are generated by the JINR Phasotron proton accelerator, which can provide a current of maximum 3.2 μA. In the following study, a beam power of 2.0 kW, corresponding to a current of 3.0 μA ($1.9 \cdot 10^{13}$ protons/s), was assumed in all simulations. For the calculated effective multiplication coefficient (k_{eff} ~0.95), this proton beam induces a total core power of about 60 kW. In Fig. 1, a schematic view of the target, the core, the reflector and the upper part of the biological shielding is depicted. The core is surrounded by a lead reflector, which is 30 cm thick in the axial directions. In the present SAD design, the biological shielding above the reactor consists of a 100 cm thick section of heavy concrete, followed by 340 cm of standard concrete (the elementary compositions of the concrete materials are displayed in Table 1). Since the particles that leak out radially from the reflector do not contribute significantly to the effective dose at the top of the shielding, the radial and the lower sections of the shielding have been neglected in the simulations.

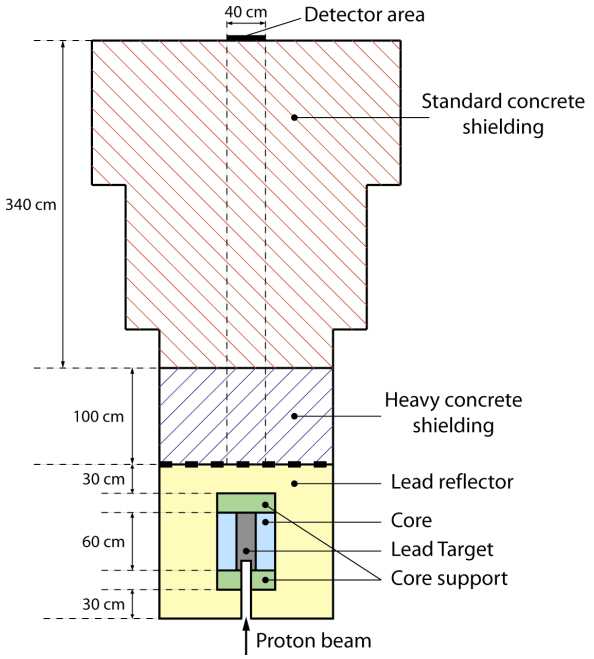

Fig. 1. Schematic rz-view of the present design of the SAD reactor system, including the target, the core, the lead reflector and the upper part of the biological shielding. The shielding consists of a 100 cm thick section of heavy concrete plus 340 cm of standard concrete. The effective dose was calculated at the detector area at the upper surface of the biological shielding.

Table 1
Elementary composition of the standard and the heavy concrete used in the biological shielding above the SAD core [17].

Element	Standard concrete (wt%)	Heavy concrete (wt%)
O	53.0	14.6
Si	37.2	4.4
Ca	8.3	4.6
H	1.0	0.6
Mg	0.5	2.7
Fe	-	66.3
C	-	2.5
S	-	1.5
Ni	-	0.7
Mn	-	0.7
Cr	-	0.5
Al	-	0.5
P	-	0.2
Density (g/cm^3)	2.30	4.44

3.2. Calculation Method

In order to determine the total effective dose, the flux of the particles that leak out at the detector area at the top of the biological shielding was calculated with the high-energy Monte Carlo code MCNPX (version 2.5.e), with the energy spectrum divided into the appropriate energy bins. Knowing the flux, $\Phi_{E,P}$, and the fluence-to-effective dose conversion coefficients, $(E/\Phi)_{E,P}$, for each energy bin and each particle type, the total effective dose per unit time, E, can then be determined as

$$E = \sum_P \left(\sum_E (E/\Phi)_{E,P} \cdot \Phi_{E,P} \right). \qquad (4)$$

The summation is over all energy bins and all particles. MCNPX was used in coupled neutron, proton and photon mode and the evaluated nuclear data library used in the simulations was LA150 [18] for those isotopes included in this library and ENDF/B-6.8 for the remaining isotopes. The high-energy physics package used by MCNPX was the Bertini model [19].

The main objective of the present study has been to determine the effective dose induced at the top of the biological shielding. For practical reasons, the simulations were divided into two steps. In the first simulation, where the 660 MeV source protons impinge on the spallation target, only the target, the core and the reflector were present. The properties, in terms of position, direction and energy, of the particles that leak out from the upper surface of the reflector (marked with the thick dotted line in Fig. 1) were recorded and written to a source file. In the second step, in which only the shielding was present, these particles were re-emitted as fixed source particles in a separate run and transported through the shielding. The particle fluxes and the effective dose were then deter-

mined at the detector area at the top of the shielding (marked with the thick black line at the top of Fig. 1).

In Monte Carlo-based shielding calculations, different kinds of variance reduction techniques are generally needed in order to obtain reliable statistics within reasonable computing time. In the present study, the Geometry splitting with Russian roulette option in MCNPX was applied. The biological shielding was divided into separate layers with increasing splitting multiplicity, such that the particle populations remained approximately constant from the source point to the detection point. The thickness of each layer was 10 cm and, since the particle fluxes decrease approximately logarithmically with the distance travelled, the importance between two neighbouring layers was increased by a nearly constant factor.

4. Results and discussion

4.1. The radiation fields at the reflector surface

From the target-core-reflector simulation, it was found that the flux of the neutrons at the centre (within 20 cm radius) of the upper reflector surface, is about $3.5 \cdot 10^{10}$ $cm^{-2}s^{-1}$ (Table 2). Most of these neutrons come from the fission multiplication in the core and have an energy distribution peaking at about 500 keV (Fig. 2). However, there is a small fraction of the neutrons that come directly from the spallation process in the target and carry very high energy. Although the fraction of neutrons with energy higher than 10 MeV is only ~0.12%, it will be shown below that these high-energy neutrons contribute for the entire part of the radiation fields and the effective dose at the top of the shielding.

The fluxes of photons and protons at the reflector surface were, as expected, significantly lower than the neutron flux, in the order of $8 \cdot 10^7$ and $4 \cdot 10^5$ $cm^{-2}s^{-1}$, respectively. The major part of the photons was found in the energy range between 0.1 MeV and 10 MeV, while most of the protons had energy higher than 10 MeV.

Table 2
Flux (Φ) of neutrons, photons and protons and the relative fractions of particles in different energy intervals, that leak out through the center of the upper reflector surface (averaged over a 20 cm radius).

	Φ	Fraction of particles in different energy bins (%)			
	($cm^{-2}s^{-1}$)	0-1 MeV	1-10 MeV	10-100 MeV	100-660 MeV
Neutrons	$3.5 \cdot 10^{10}$	95.4	4.4	0.08	0.04
Photons	$8.1 \cdot 10^7$	57.2	42.8	0	0
Protons	$4.0 \cdot 10^5$	0	5	60	35

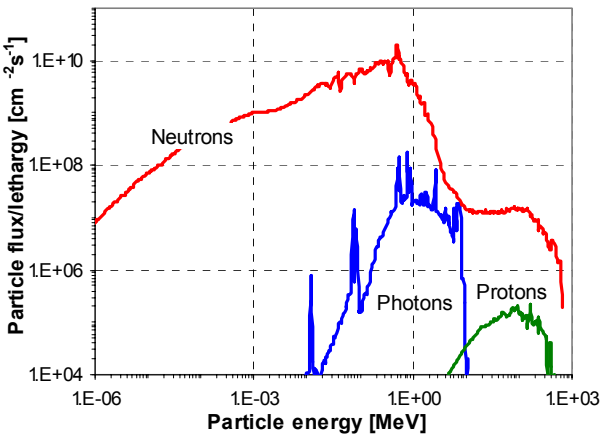

Fig. 2. Energy spectra of the neutrons, photons and protons that leak out through the centre (within 20 cm radius) of the upper reflector surface. The resolution of the spectra corresponds to a constant lethargy width of 0.05.

4.2. The radiation fields at the top of the biological shielding

4.2.1. Effective dose

The separate fluxes for neutrons, photons and protons calculated at the detector area at the top of the biological shielding, as well as the corresponding effective doses and the total effective dose, are displayed in Table 3. The total effective dose was found to be about 190 μSv/h, with a statistical uncertainty of about 5%. According to radiation protection rules in Russia, the maximal allowed effective dose for civil personnel is 12 μSv/h. However, provided that access for working personnel to the rooms above the shielding will be prohibited during operation, the radiation dose obtained for the present design of the biological shielding is in agreement with the radiation regulations.

Table 3
Separate flux (Φ) and effective dose (E) of neutrons, photons and protons, as well as the total effective dose, at the detector area at the top of the biological shielding.

Neutrons		Photons		Protons		Total	
Φ ($cm^{-2}s^{-1}$)	E (μSv/h)	Φ ($cm^{-2}s^{-1}$)	E (μSv/h)	Φ ($cm^{-2}s^{-1}$)	E (μSv/h)	E (μSv/h)	1σ-error (%)
174	172	114	1.9	2.0	18	192	~5

Apparently, the neutrons contribute for the major part of the effective dose, ~89%, but, a non-negligible part of the effective dose is also induced by photons and protons, which contribute for ~1% and ~10%, respectively. The reason why the contribution from photons is only 1%, although the fluxes of neutrons and photons are in the same order of magnitude, is that the conversion coefficients of the photons (having energy between 0.1 and 10 MeV) are about 100 times smaller than those of the neutrons (a major fraction having energy around 100 MeV). Similarly, the conversion coefficients for the protons (with the major part having energy around 100 MeV) are about 10 times higher than those for the neutrons, which explains the relatively high contribution to the effective dose induced by the much lower flux.

The explanation to why there is such a considerable flux of photons and protons detected, although only high-energy neutrons entering into the concrete are expected to penetrate the entire shielding, is that the high-energy neutrons create, apart from secondary neutrons with lower energy, also secondary photons and protons. The high-energy neutrons will thus be followed through the concrete by cascades of neutrons, photons and protons. Hence, all protons and photons detected at the top of the shielding have been created by neutrons inside the standard concrete. The minimum energy of neutrons required to create protons is in the order of a few MeV, while thermal neutrons have the highest probability to create photons. Since both photons, protons and low-energy neutrons have limited range in the concrete, it can moreover be assumed that the major part of the detected particles have been created nearby the detector area.

4.2.2. Energy spectra

The energy distributions of the neutrons, photons and protons detected at the top of the biological shielding are displayed in Fig. 3. It was found that about half of the neutrons have energy above 10 MeV. Accordingly, since the neutrons contribute for the major part of the effective dose and since the conversion coefficients increases with energy, the major part of the total effective dose is induced by neutrons with energy higher than 10 MeV.

The energy spectrum of the detected neutrons is typical for a high-energy proton beam shielded by concrete. The shape of these spectra is generally characterized by a thermal peak, an evaporation shoulder around a few MeV and a high-energy spallation peak, which is indeed the case. The high-energy peak with a maximum at about 100 MeV arises mainly from the deeply penetrating neutrons that were emitted in the intranuclear cascade reactions in the spallation target. The major part of these high-energy neutrons, formed in direct head-on collisions between the incident source protons and the individual target nucleons, were emitted in the forward direction and have been transported through the shielding without being significantly moderated. Since only the most energetic neutrons can be traced back to the shielding region of heavy concrete, the detected spectra below about 100 MeV is determined only by the isotopic composition of the standard concrete. The evaporation shoulder comes from the neutrons emitted in the neutron-induced spallation reactions on the heavier elements in the standard concrete (mainly oxygen and silicon). The narrow peak on top of this shoulder, located at 2.35 MeV, is the result of a deep minimum in the elastic scattering cross-section of ^{16}O.

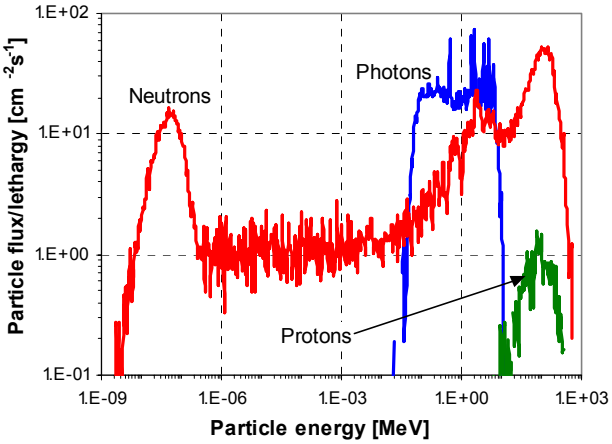

Fig. 3. Energy spectra of the neutrons, photons and protons detected at the top of the concrete shielding. The resolution of the spectra corresponds to a constant lethargy width of 0.05.

Most of the detected photons have been created in neutron-induced reactions, by either one of the two following type of reactions. In the first type, a high-energy neutron is scattered on one of the concrete nuclei and transfers a considerable amount of energy to it, leaving it in an excited state. When the nucleus is de-excitated, photons of various discrete energies are emitted. The second type of reaction that leads to photon production is a neutron-capture reaction. Examples of such reactions occurring in the concrete are $^{16}O(n,\gamma)^{17}O$ and $^{28}Si(n,\gamma)^{29}Si$ with Q-values of 4.1 MeV and 8.5 MeV, respectively. Thermal neutrons have the highest probability of inducing this type of reaction. The overall photon energy spectrum, ranging mainly from about 0.1 MeV to about 10 MeV, can be characterized by a Compton continuum on top on which is added hundreds of discrete photon peaks of varying intensity. Among the most distinct peaks can be mentioned

those originating from electron-positron annihilation (0.511 MeV), the formation of ^{2}H (fusion of a neutron and a proton emitting a photon carrying the released binding energy of 2.225 MeV), gamma emission following neutron capture in ^{28}Si (4.935 MeV) and the de-excitation of $^{16}O^{*}$ (6.130 MeV).

The shape of the proton energy spectrum is similar to that of the high-energy neutrons, the major part having energy higher than 10 MeV. The protons have been created in direct head-on reactions between the high-energy neutrons and the various nuclei in the standard concrete. In this type of reactions, a large fraction of the neutron energy is transferred to the released proton, which is emitted preferably in the forward direction.

4.3. Attenuation in the biological shielding

In order to estimate the range of the particles transported in the biological shielding, the attenuation of parallel beams of neutrons, photons and protons of various discrete energies have been studied. The attenuation of a beam of non-charged monoenergetic particles in a homogeneous material can be expressed by the following relation [20];

$$N/N_0 = B(x)\cdot e^{-\mu x}, \qquad (5)$$

where N/N_0 refers to the relative intensity of the beam, $B(x)$ is the build-up factor and μ is the linear attenuation coefficient. The build-up factor represents the ratio of the intensity of the total radiation reaching a point, to the intensity of the primary radiation reaching the same point. If the incident beam, as well as the area one is trying to shield, would be very narrow, or, if the shielding material would be very thin, only the unscattered primary particles would contribute to the effective dose and B would be equal to unity. However, since this is rarely the case, B will in general be larger than 1, as it accounts also for the contribution coming from those particles that have been scattered and from those that have been formed by the primary particles. It should be noted that, for beams of mixed energies, the decay of the total intensity have to be described by more than one exponential.

In this study, the attenuation length is defined as the thickness required to reduce the effective dose by a factor of 10 (the tenth-value thickness), and will be labelled λ_{10} ($\lambda_{10} = \ln(10)/\mu$). The attenuation of the effective dose is approximately equal to the diminishing of the flux. The attenuation coefficients and the attenuation lengths, displayed in Table 4, were obtained by simulating the transport of parallel mono-energetic particle beams through a slab of concrete and calculating the effective dose at different distances from the incident point. All particles contributing to the effective dose were included, i.e., apart from the primary source particles, also the neutrons, photons and protons that are formed as the primary particles are moderated. An exponential function was then fitted to the data points and μ was determined as the slope of the decay curve. So-called attenuation factors have also been determined for the mono-energetic particle beams impinging on the SAD shielding (100 cm of heavy concrete plus 340 cm of standard concrete), referring to the ratio of the effective dose at the incident point to the effective dose at the top of the shielding.

4.3.1. Attenuation of mono-energetic neutron beams

It is shown in Table 4 and Fig. 4 that the attenuation length of neutrons transported in concrete increases considerably with increasing energy. For instance, the attenuation length of a 100 MeV neutron beam is about three times longer than for a 10 MeV neutron beam and the attenuation factor for the present SAD design is in the order of 10^{17} for the 10 MeV neutrons, whereas only about 10^{5} for the 100 MeV neutrons. These results indicate that the contribution to the effective dose above the SAD shielding from neutrons below 10 MeV will be negligibly small (this assumption will be verified below by direct MCNPX simulations). As can be seen in Fig. 4, the attenuation of the neutron beams does not decay exponentially during the first part of the concrete slab (the build-up factor is larger than 1 and increases with the thickness). As was explained above, the attenuation of the unscattered primary neutrons will be purely exponential (no build-up factor needed), but, in particular the 100 MeV neutrons, will create secondary particles as they are moderated. These particles, mainly the neutrons, will contribute considerably to the effective dose close to the incident point. However, as they have comparatively low energy and limited range in the concrete, the primary high-energy neutrons will dominate the attenuation completely at longer distances. When the energy distributions of the particles contributing to the effective dose reach their equilibrium, i.e. only the amplitudes and not the shape of the spectra change, the total effective dose will decay with the same single exponential as the incident primary neutrons. For distances beyond about 50 cm and 100 cm, for the 10 MeV neutrons and the 100 MeV neutrons, respectively, the energy spectra are in equilibrium and the decay constants have reached their asymptotic value of a single exponential (the build-up factor is constant). The calculated data beyond these points have been used to determine the attenuation coefficients and the attenuation lengths of the neutron beams.

Table 4
Attenuation lengths (λ_{10}) for the decay of the effective dose, induced by parallel mono-energetic beams of neutrons, photons and protons of different energies impinging on thick slabs of either heavy or standard concrete. So-called attenuation factors have been calculated for the mono-energetic particles impinging on the SAD shielding (100 cm of heavy concrete plus 340 cm of standard concrete) and refer to the ratio of the effective dose at the incident point to the effective dose at the top of the shielding.

Particle type	Energy (MeV)	Attenuation length, λ_{10} (cm)		Attenuation factor
		Heavy concrete	Standard concrete	
Neutrons	1	13	16	$2.4 \cdot 10^{23}$
	10	18	29	$1.4 \cdot 10^{17}$
	100	54	92	$2.6 \cdot 10^{5}$
	500	74	135	$3.3 \cdot 10^{3}$
Photons	1	9	17	$>10^{30}$
	10	21	49	$1.5 \cdot 10^{12}$
Protons	100	39	51	$4.1 \cdot 10^{10}$
	500	68	111	$2.2 \cdot 10^{5}$

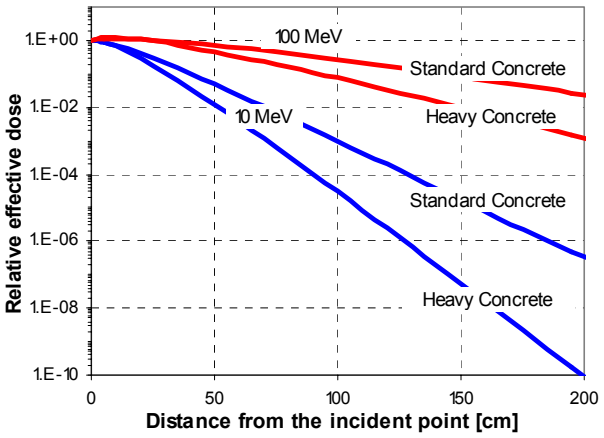

Fig. 4. Relative effective dose as a function of distance from the incident point, in standard and heavy concrete for parallel beams of 10 MeV and 100 MeV neutrons. The effective dose includes the contributions from all secondary particles, i.e. the neutrons, photons and protons that are created when the incident high-energy neutrons are moderated.

4.3.2. Attenuation of mono-energetic photons beams

Photons in the energy range where most of the reflector leakage photons are found (0.1 to 10 MeV) have comparatively short range in the concrete, in the same order of magnitude as neutrons of similar energy. Therefore, the photons that leak out through the reflector surface can be assumed to give zero contribution to the effective dose at the top of the shielding, which can also be understood from the large attenuation factors shown in Table 4. The build-up factors are closer to 1 than for the neutron beams, as the photons form less secondary particles, and the attenuation curves become purely exponential already very close to the impact position.

4.3.3. Attenuation of mono-energetic proton beams

Opposite to neutrons and photons, protons carry electric charge. Therefore, the attenuation of a proton beam shows a more complicated behaviour than the exponential decay described by Eq. 5. When a high-energy proton is moderated in a material, the rate of energy loss increases as the proton energy decreases. Near the end of the path, when most of its energy has been lost, the energy loss per unit distance reaches a maximum (the Bragg peak), after which it drops to zero as the particle comes to rest. This abrupt slowing down enables a precise range of the incident protons to be defined. For instance, the typical range of 500 MeV protons in the heavy concrete in the SAD shielding was found to be about 35 cm, which is illustrated in Fig. 5. Hence, protons have very limited range in concrete, compared to neutrons of similar energy. The typical range of the 100 MeV protons is only a few cm.

However, the high-energy protons being transported in the concrete will create spectra of secondary particles as they interact with the concrete nuclei. Some of the created neutrons will be formed in direct head-on collisions and receive the major part of the proton energy. Since these high-energy neutrons have much longer range in the concrete than the primary protons, the dominant contribution to the effective dose will after a distance longer than the typical proton range actually be induced by these secondary neutrons (Fig. 5). Moreover, as was already explained, these high-energy neutrons will, in their turn, create spectra of both neutrons, photons and protons. Hence, at distances longer than the primary proton range, the attenuation of the effective dose directly induced by protons, as well as that by photons, will decay with the same exponential as the neutrons. It can thus be concluded that the effective range of high-energy protons incident on a concrete shielding, in terms of inducing effective dose, is determined mainly by the attenuation of neutrons with similar energy and is much longer than can be expected from studying only the Bragg curve of the incident protons. This is also illustrated in Table 4, where the attenuation lengths for the protons have been determined from the

exponential neutron decay beyond the Bragg peak. It is seen that the attenuation lengths for the protons are only slightly shorter than for the neutrons of the same energy.

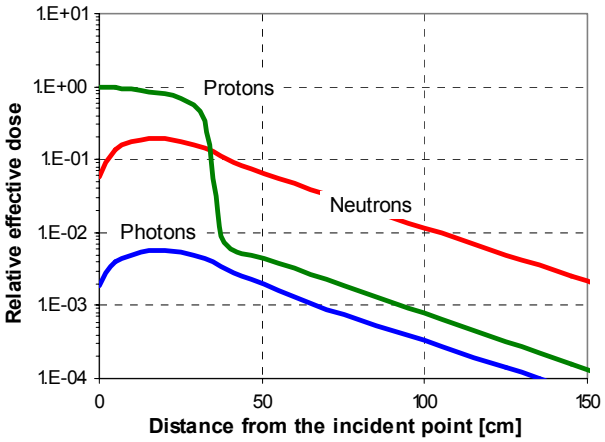

Fig. 5. Attenuation of the effective dose in heavy concrete for parallel beams of 500 MeV protons. The different curves represent the separate contributions to the effective dose from protons, neutrons and photons.

However, despite the relatively long range of the proton-induced effective dose, the rapid decrease of the total effective dose at the Bragg point reduces the contribution to the dose at the top of the SAD shielding significantly. Moreover, the intensity of the proton flux at the reflector surface is very low (more than 100 times lower than for the high-energy neutrons), which makes the relative contribution to the effective dose from the protons negligible.

4.3.4. Attenuation of the SAD-leakage particles in the biological shielding

In the following sub-section, the effective dose induced by the particles leaking out from the SAD reactor system has been studied in the biological shielding as a function of the distance from the reflector-shielding boundary. In Fig. 6, it is shown that, during the first ~50 cm in the heavy concrete, the decay of the effective dose is very fast and cannot be described by a single exponential. The reason for this is that the effective dose close to the reflector is induced mainly by the low-energy neutrons leaking out from the reflector, which have a large variety in energy. Since neutrons with different energy are attenuated at different rates, the total decay will be described by the sum of many exponentials. However, all of these low-energy neutrons are efficiently attenuated in the heavy concrete and, beyond about half a meter, the decay of the effective dose is largely dominated by the attenuation of the high-energy neutrons. The particle spectra have almost reached their equilibrium and the decrease of the effective dose is very close to exponential. However, entering into the standard concrete, the decay switches into another mode, with less efficient attenuation. Since the energy spectra of the transported particles changes at this boundary, some distance is required before the decay curve becomes single-exponential again.

In order to determine the linear attenuation coefficients and the attenuation lengths in the two shielding materials, two exponential curves have been fitted to the MCNPX-calculated data points, one for the heavy concrete and one for the standard concrete. In the heavy concrete, the purely exponential decay appears first after about 150 cm (although it is close to exponential already after 50 cm), so additional simulations, extending the heavy concrete, had to be performed to determine the attenuation coefficient (data points from 150 to 250 cm were used for the curve fitting). In the standard concrete, the equilibrium of the particle spectra is reached after a few tenths of cm from the boundary and the data points from 150 to 400 cm were used for the curve fitting. The attenuation lengths (λ_{10}) of the effective dose obtained from the exponential fits were found to be 58 cm in heavy concrete and 93 cm in standard concrete (Table 5).

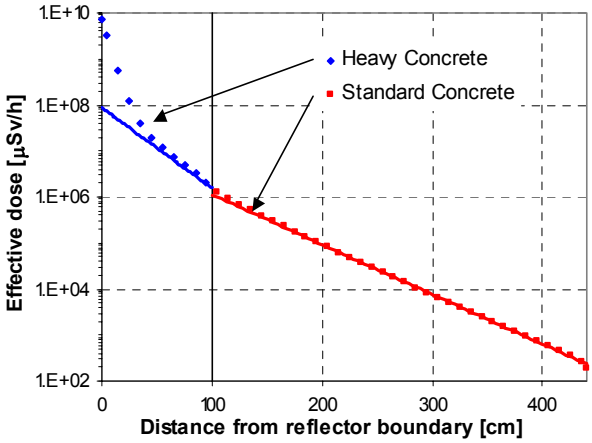

Fig. 6. Total effective dose induced by the particles leaking out from the SAD reactor system as a function of the distance from the reflector-shielding boundary. Exponential curves have been fitted to the MCNPX-calculated values; one in the heavy concrete and one in the standard concrete.

Table 5
Attenuation lengths (λ_{10}) and attenuation factors for the decay of the effective dose induced by the particles leaking out from the SAD reactor system.

Attenuation length, λ_{10} (cm)		Attenuation factor
Heavy concrete	Standard concrete	
58	93	$3.9 \cdot 10^7$

4.4. Contribution to the effective dose from source neutrons in different energy intervals

As was shown above, low-energy neutrons have very short attenuation lengths in concrete, compared to high-energy neutrons, which indicates that only the high-energy neutrons have long enough range to penetrate the full length of the shielding and to induce any significant effective dose at the top of it. In order to calculate the separate contributions to the effective dose from neutrons of differ-

ent energies, the flux of the neutrons entering into the biological shielding from the reflector was divided into four energy bins (0-1, 1-10, 10-100 and 100-660 MeV). As expected, the relative contribution from the two low-energy bins is zero (Table 6). The contribution from the third energy bin (10-100 MeV) is also limited (~0.3%), whereas the last energy bin (100-660 MeV) contributes for nearly the entire part of the effective dose. It was also found that the contributions from photons and protons are negligible. As was explained above, the dose originating from the source protons is induced by the secondary neutrons created as the protons are moderated in the heavy concrete.

The maximal energy of the neutrons released in the fission processes in the reactor core is in the order of 10 MeV. It can therefore be assumed that the entire part of the effective dose detected at the top of the shielding originates from the proton-induced spallation reactions in the target and practically nothing from the fission multiplication in the core. Thus, it can be concluded that the effective dose is directly proportional to the proton beam power and that it is independent of the reactivity and the total power of the sub-critical core.

Table 6
Relative contribution to the total effective dose originating from the source particles that enter into the biological shielding from the reflector. The neutrons were divided into four different energy intervals.

Source particle	Energy interval (MeV)	Relative contribution to E
Neutrons	0-1	0 (~10^{-18})
	1-10	0 (~10^{-14})
	10-100	0.3%
	100-660	99.7%
Photons	All	0 (~10^{-12})
Protons	All	0.01%

4.5. Optimising the design of the biological shielding

4.5.1. Reducing the effective dose to Russian regulation limits for working personnel

As was mentioned above, the effective dose obtained for the present design of the biological shielding above the SAD core (~190 μSv/h) meets the Russian regulations for radiation doses. However, if the access for working personnel in the rooms above the reactor would be required, the effective dose would have to be decreased to 12 μSv/h, which is about 15 times lower than for the present design. In such case, the shielding would have to be modified, for instance by increasing the fraction of heavy concrete in the shielding.

The amount of standard concrete that must be replaced by heavy concrete in order to obtain the desired dose can be determined in two ways, either by extrapolating the two exponential functions that were fitted to the MCNPX-calculated data (Fig. 6) or by direct MCNPX calculations. Applying the extrapolation method, it was found that the boundary between the heavy concrete and the standard concrete should be located at 316 cm from the reflector, in order to reduce the dose to 12 μSv/h. In the second method, the effective dose was calculated in different MCNPX-simulations with the boundary between the heavy concrete and the standard concrete varying. Interpolating between the obtained data points, it was found that the desired dose is obtained with the boundary located at 305 cm, which is in fairly good agreement with the first result. The main reason for the slight disagreement between the two results is that the attenuation is not purely exponential during the first tenths of cm in the standard concrete, which was not taken into account in the extrapolation method.

4.5.2. Shielding thickness required for a large-scale ADS

The power of the proton beam in the SAD experiments is relatively low (maximum 2 kW) and not representative of a future large-scale ADS, which might require a beam power of several MW. The thickness of concrete required to maintain the dose at 12 μSv/h for different beam powers have been estimated by calculating the effective dose as a function of concrete thickness, for heavy concrete and standard concrete separately, and then extrapolating the results to the required thickness. Since the effective dose is linearly proportional to the beam power (given a fix proton energy), the amount of extra concrete required for an increase of the beam power by a factor of 10 is equal to the attenuation length, λ_{10} (58 cm for heavy concrete and 93 cm for standard concrete). In Table 7, the amount of standard concrete and heavy concrete, respectively, required to maintain the effective dose at 12 μSv/h is displayed for the proton beam power varying from 2 kW to 20 MW.

Table 7
Thickness of the biological shielding required to maintain the effective dose at 12 μSv/h for a proton beam power varying from 2 kW to 20 MW. The shielding consisted of only heavy concrete or only standard concrete, except for the 2 kW proton beam, where the two materials were also combined.

Beam power (kW)	Heavy concrete (cm)		Standard concrete (cm)
2.0[A]	305	+	135
	394		591
20	453		684
200	511		777
$2.0 \cdot 10^3$	570		869
$20 \cdot 10^3$	628		962

[A] The desired effective dose for a proton beam power of 2 kW could be obtained either by combining 305 cm of heavy concrete plus 135 cm of standard concrete, or by using 394 cm of only heavy concrete or 591 cm of only standard concrete.

4.5.3. Lead or iron as high-energy neutron shield

Heavier elements, like lead, generally have high cross-sections for inelastic reactions of high-energy neutrons and can therefore be assumed to be an efficient shielding of high-energy neutrons. However, as the neutrons are attenuated, there is a considerable build-up of low-energy neutrons that will dominate the contributions to the effective dose. For this reason, lead could not be used as shielding alone, but might, if followed by a layer of some hydrogenous material, such as concrete, significantly improve the overall shielding properties. Iron is also a material known for having favourable shielding features, but with similar properties as lead of producing low-energy neutrons. The microscopic cross-sections for high-energy neutrons in iron are lower than in lead, but the atomic density is higher by a factor of 2.5. Therefore, iron can actually be expected to attenuate the high-energy neutrons more efficiently than lead.

In order to verify these assumptions and with the aim of providing a proposal of an improved biological shielding at the SAD facility, the effective dose was calculated with the 100 cm thick section of heavy concrete replaced by iron and lead, respectively. Indeed, it is shown in Table 8 that iron improves the shielding capacity more than lead, reducing the effective dose by more than a factor of 8, compared to the present shielding design. Other ways of improving the shielding capacity might be to combine layers of iron or lead with different types of hydrogenous materials.

Table 8
Separate flux (Φ) and effective dose (E) at the top of the biological shielding, with the 100 cm thick section of heavy concrete replaced by iron or lead. The 340 cm of standard concrete was not changed.

	Neutrons		Photons		Protons		Total
	Φ ($cm^{-2}s^{-1}$)	E (μSv/h)	Φ ($cm^{-2}s^{-1}$)	E (μSv/h)	Φ ($cm^{-2}s^{-1}$)	E (μSv/h)	E (μSv/h)
Fe	21	21	14	0.2	0.2	1.9	23
Pb	30	30	18	0.3	0.5	5.0	36

5. Conclusions

The main objective of the present paper was to determine the effective dose above the biological shielding covering the upper part of the SAD core. The sub-critical core, loaded with fast-reactor MOX fuel, is driven by a 660 MeV proton beam of 3.0 μA current (2.0 kW), impinging on a spallation target of lead. The high-energy neutrons created in the spallation process are deeply penetrating in all shielding materials and constitute a major concern in shielding design studies. Consequently, the biological shielding around an ADS, even for those operating at comparatively low power, must be made thicker and much more efficient than those typically needed for critical reactors. In the present SAD design, the biological shielding consists of 100 cm of heavy concrete plus 340 cm of standard concrete.

In order to determine the effective dose, the fluxes of the particles leaking out through the top of the shielding were first calculated with the high-energy Monte Carlo code MCNPX. By combining appropriate fluence-to-effective dose conversion coefficients with the calculated fluxes, the effective dose could then be obtained. The total effective dose at the centre of the top of the shielding was found to be about 190 μSv/h. This dose is in agreement with the radiation protection regulations in Russia, provided that access by working personnel to this area is prohibited during operation. The major part of the dose is induced by neutrons (89%), whereas the rest by protons (10%) and photons (1%). The spectrum of the detected neutrons can be characterised by a thermal peak, an evaporation shoulder at a few MeV and a strong high-energy peak centred around 100 MeV. Since more than half of the neutrons have energy higher than 10 MeV and since the conversion coefficients increases with energy, the high-energy neutrons contribute for the major part of the effective dose.

The attenuation of the effective dose was studied as a function of shielding thickness. After the composite decay during the first tenths of cm in each concrete shielding material, the dose was found to decrease exponentially, following one exponential in the heavy concrete and one in the standard concrete. By fitting exponential functions to the calculated data points, the attenuation lengths were determined for the two concrete materials. These exponential functions were also used for estimating the extra amount of heavy and standard concrete needed to reduce the dose to the Russian limit for working personnel (12 μSv/h) or to increase the proton beam power to values representative for a large-scale ADS without increasing the dose.

Moreover, the relative contributions to the effective dose from low-energy neutrons and high-energy neutrons that leak out from the reactor were determined. The fact that 100% of the dose originates from neutrons with energy higher than 10 MeV, which are exclusively produced in the spallation target, shows that the effective dose at the top of the SAD shielding is directly proportional to the proton beam power and that it is independent of the total power and the reactivity of the sub-critical core. Finally, the heavy concrete in the biological shielding was replaced by lead and iron, in order to optimise the shielding of the high-energy neutrons. Of the two, it was found that iron is the most efficient shielding material, reducing the effective dose by a factor of 8, compared to the present shielding design.

6. Acknowledgements

This work was partially supported by SKB AB (Swedish Nuclear Fuel and Waste Management Co) and the Swedish Centre for Nuclear Technology. The development of the SAD design is financed by the International Science and Technology Centre (ISTC).

7. References

1 W. Gudowski, A. Polanski, I. V. Puzynin, V. Shvetsov, "*Monte Carlo modeling of a sub-critical assembly driven with the existing 660 MeV JINR Proton Accelerator*", Int. Meeting AccApp'01, November 11-15, 2001, Reno, Nevada, USA (2001).

2 ISTC Project 2267. http://www.tech-db.ru/istc/db/projects.nsf/prjn/2267

3 M. Salvatores et al., "*Long-lived radioactive waste transmutation and the role of accelerator driven (hybrid) systems*," Nucl. Instrum. Methods A, **414**, 5 (1997).

4 D. G. Foster, "*Review of PNL study on transmutation processing of high level waste*," LA-UR-74-74, Los Alamos National Laboratory (1974).

5 T. Takizuka, "*Conceptual design of transmutation plant*," Proc. Specialist Mtg. Accelerator Driven Transmutation Technology for Radwaste, LA-12205-C, p. 707, Los Alamos National Laboratory (1991).

6 L. S. Waters, "*MCNPX™ User´s Manual – Version 2.1.5*," Los Alamos National Laboratory, November 14, (1999).

7 International Commission on Radiation Protection, "*Conversion coefficients for use in radiological protection against external radiation*," ICRP Publication 74, Pergamon Press, Oxford (1997).

8 International Commission on Radiation Units and Measurements, "*Conversion coefficients for use in radiological protection against external radiation*," ICRU Report 57, Bethesda, Maryland (1998).

9 S. Leray et al., "*Spallation Neutron Production by 0.8, 1.2, and 1.6 GeV Protons on various Targets*," *Phys. Rev.*, **C65** (2002).

10 I. Koprivnikar, E. Schachinger, "*The biological shield of a high-intensity spallation source: a Monte Carlo design study*", Nucl. Instr. Meth. In Phys. Res. A487, 571-584, (2002).

11 P. Seltborg, et al, "*Investigation of Radiation Fields outside the Sub-critical Assembly in Dubna*", International Conference on Radiation Shielding ICRS-10, May 9-14 2004, Funchal, Madeira Island, Portugal (2004).

12 International Commission on Radiation Protection, "*Recommendations of the international commission on radiological protection*," ICRP Publication 60, Pergamon Press, Oxford (1991).

13 W. S. Snyder et al., "*Estimates of absorbed fractions for monoenergetic photon sources uniformly distributed in various organs of a heterogeneous phantom*," MIRD Pamphlet No. 5. Society of Nuclear Medicine, New York (1969).

14 R. Kramer et al., "*The calculation of dose from external photon exposures using reference human phantoms and Monte Carlo methods. Part I: the male (ADAM) and female (EVA) adult mathematical phantoms*," GSF-Bericht S-885. Gesellschaft für Strahlen-und Umweltforschung mbH, Munich, Germany, (1982).

15 V. Mares, H. Schraube, "*The effect of the fluence to dose conversion coefficients upon the dose estimation to cosmic radiation*, " Expert Group on Shielding Aspects of Accelerators, Targets and Irradiation Facilities (Sixth Meeting - SATIF-6), April 10-12, 2002, Menlo Park, USA (2002).

16 M. Pelliccioni, "*Overview of fluence-to-effective dose and fluence-to-effective dose equivalent conversion coefficients for high-energy radiation calculated using the FLUKA code*," Radiat. Prot. Dosim. **88**, 279-297, (2000).

17 Internal SAD document at the Joint Institute for Nuclear Research (JINR).

18 M. B. Chadwick et al., *Nucl. Sci. Eng.* (submitted 1998, Los Alamos National Laboratory LA-UR-98-1825 (1998)).

19 H. W. Bertini, Phys. Rev. 131 (1963) pp 1801.
H. W. Bertini, Phys. Rev. 188 (1969) pp 1711.

20 J. K. Shults, R. E. Faw, "*Radiation Shielding*", Prentice Hall PTR, Upper Saddle River, NJ, (1996).

Table A.1
Effective dose per unit fluence (E/Φ) for neutrons, photons and protons (ISO geometry) used in the present study. The conversion coefficients for neutrons in the energy range from $1 \cdot 10^{-9}$ MeV to 20 MeV are taken from [8], while the coefficients for neutrons from 30 to 500 MeV, as well as all coefficients for photons and protons, are taken from [15].

Neutrons		Photons	
Energy (MeV)	E/Φ [pSv·cm^2]	Energy (MeV)	E/Φ [pSv·cm^2]
1.E-09	2.40	0.02	0.093
1.E-08	2.89	0.05	0.21
2.5E-08	3.30	0.1	0.31
1.E-07	4.13	0.2	0.61
2.E-07	4.59	0.5	1.65
5.E-07	5.20	1	3.30
1.E-06	5.63	2	6.02
2.E-06	5.96	5	12.15
5.E-06	6.28	10	20.63
1.E-05	6.44	20	32.40
2.E-05	6.51	50	62.16
5.E-05	6.51	100	96.63
1.E-04	6.45	200	133.5
2.E-04	6.32	500	190.2
5.E-04	6.14		
1.E-03	6.04	Protons	
2.E-03	6.05	10	20.6
5.E-03	6.52	20	173.9
0.01	7.70	30	423.8
0.02	10.2	50	1346.0
0.03	12.7	100	2953.8
0.05	17.3	150	4648.0
0.07	21.5	200	4577.4
0.1	27.2	300	3445.6
0.15	35.2	500	2965.6
0.2	42.4		
0.3	54.7		
0.5	75.0		
0.7	92.8		
0.9	108		
1	116		
1.2	130		
2	178		
3	220		
4	250		
5	272		
6	282		
7	290		
8	297		
9	303		
10	309		
12	322		
14	333		
15	338		
16	342		
18	345		
20	343		
30	356		
50	389		
100	412		
150	527		
200	526		
500	791		